Observations of hyperon-nucleus systems produced on ^{12}C and ^{7}Li targets using the (K^-,π^+) reaction at 715 MeV/c

L. Tang, E. Hungerford, T. Kishimoto, B. Mayes, and L. Pinsky
University of Houston, Houston, Texas 77004

S. Bart, R. Chrien, P. Pile, and R. Sutter
Brookhaven National Laboratory, Upton, New York 11973

P. Barnes, G. Diebold, G. Franklin, D. Hertzog, B. Quinn, J. Seydoux, and J. Szymanski
Carnegie Mellon University, Pittsburgh, Pennsylvania 15213

T. Fukda
Osaka University, Osaka, Japan

R. Stearns
Vassar College, Poughkeepsie, New York 10001
(Received 14 March 1988)

The hypernuclear systems $\Sigma^- + {}^{11}B$ and $\Sigma^- + {}^{6}He$ were produced by the (K^-,π^+) reaction on targets on ^{12}C (graphite) and ^{7}Li using 715 MeV/c incident kaons. Spectra were measured at reaction angles of 4° and 12° to investigate the momentum transfer dependence. A decay detector surrounded the target to provide a decay mode tag. Data were analyzed with and without this tag. The resulting spectra for the ^{12}C target are similar to previous results with the exception that the narrow structure reported in the stopped K^- experiments is not confirmed. The spectra do show enhancements over phase space near the thresholds of the Σ plus core hole states which are created when a proton in the target is converted into a Σ. The decay mode cut shows a correlation between sigma-lambda conversion and this structure. No evidence of narrow states in either hypernucleus is observed in either the tagged or untagged data.

I. INTRODUCTION

The (K,π) reaction has been successfully applied to the production of valence Λ hypernuclear states for some time. This reaction is interpreted in terms of a one-step process which changes a neutron in the nucleus into a Λ (neutron hole-lambda particle state in the weak-coupling limit).[1] Because of the low momentum transfer involved, these Λ particles tend to populate the same shells as the neutrons they replace. In addition, since the penetrability of the K^- is low, valence levels are preferentially excited. This is in contrast to the (π,K) reaction which has been shown to populate interior hypernuclear levels.[2]

While limited in resolution, the Λ hypernuclear experiments have determined a set of Λ-N effective parameters for the $1p$ shell.[3] Thus it is quite natural to attempt to apply this reaction to Σ hypernuclei. However, a Σ placed within the nuclear medium can undergo the conversion $\Sigma N \rightarrow \Lambda N$ via the strong reaction, so that one would not expect Σ hypernuclear states to be sharply defined. Original estimates for the width of such levels range from 13 to 80 MeV.[4] For states above threshold an additional escape width contributes. Thus the report of narrow structure in the (K,π) strangeness exchange reaction on ^{9}Be near the sigma threshold has generated much theoretical and experimental excitement.[5]

Several other enhancements,[6-8] identified as sigma hypernuclei, have been experimentally studied. In particular, a recent experiment reported two narrow peaks in the $^{12}_{\Sigma}Be$ spectrum obtained from kaons stopped in a CH target.[8] These were assigned as $(p^{-1}_{3/2p}, p_{1/2\Sigma})$ and $(p^{-1}_{3/2p}, p_{3/2\Sigma})$ substitutional states. Both of these states were unbound and were observed to be $\sim$2 MeV in width. The level splitting of the structure was used to extract a sigma spin-orbit strength of 5 MeV. However, this result is not consistent with the 10-MeV strength extracted from an earlier in-flight experiment at low momentum transfer.[7]

The in-flight experiment used K momenta of 400 and 450 MeV/c in an especially designed kaon beam line at CERN. By comparing the spectra produced on C and O targets a spin-orbit strength for the Σ was assigned. A similar comparison technique was used earlier to extract the lambda spin-orbit strength.[9] Although the two experimental arrangements were quite different, there is no clear way to reconcile the very large difference in Σ spin-orbit strength extracted from the experimental spectra, other than to conclude that the interpretation of one (or both) of these spectra is incorrect.

Under the *assumption* that narrow states exist, a theoretical shell-model prediction of the $^{7}_{\Sigma}H$ spectrum has been published.[10] It shows that for a reasonable spin-

orbit strength, the level splitting between the $\frac{3}{2}^-$ and $\frac{1}{2}^-$ states is a linear function of the strength of the spin-orbit interaction. These two states are expected to be equally populated at a reaction angle of 12° for 715 MeV/c incident kaons. Using an earlier calculation of the angular distribution for the reaction,[11] ^{6}Li$(K^-,\pi^+)^6_\Sigma$H at 720 MeV/c, the ratio of $\Delta l=0$ to $\Delta l=2$ reaction strengths is predicted to be 1.4 at 4° compared to 0.2 at 12°. Thus the $p_{3/2}$ substitutional transition would be expected to dominate at small angles.

Therefore, to verify the previous structure in $^{12}_\Sigma$C, to search for bound states, and to obtain a measure of the sigma spin-orbit strength by observing the $^7_\Sigma$H spectrum, the Brookhaven National Laboratory (BNL) hypernuclear spectrometer was used with targets of C and Li to collect the experimental spectra from the (K^-,π^+) reaction near the sigma threshold.

II. EXPERIMENTAL DETAILS

This experiment was designed to (1) study the spectrum obtained from a C (graphite) target with an in-flight kaon beam and compare it to the existing data, (2) look in the appropriate mass region for bound Σ states, and (3) study the spectrum of a ^{7}Li target in an attempt to observe the splitting between the $\frac{3}{2}^-$ and $\frac{1}{2}^-$ states which is predicted to be proportional to the spin-orbit strength.[10] It was performed at Brookhaven National Laboratory's Alternating Gradient Synchrotron (AGS) using the BNL hypernuclear spectrometer[12] and low energy separated beamline I (LESBI). The beamline provided a separated kaon beam of 8×10^4 K^-/spill average intensity with a π/K ratio of approximately 8/1 at 715 MeV/c momentum. The hypernuclear spectrometer (see Fig. 1) consists of two parts: (1) a kaon spectrometer which provides momentum selection and analysis of incident kaons focused on the center of target, and (2) a pion spectrometer which analyzes at a selected angle, the momentum of the reaction pion with an angular acceptance of 15 msr, and ~3-MeV resolution for 600 MeV/c particles. The pion spectrometer can select the reaction angle from 0° (effective 4°) to 30°. A series of tracking detectors ($D1-D15$) provide particle position information for momentum analysis in both spectrometers. Each spectrometer is composed of four quadrupole magnets (Q) and a dipole magnet (D) in the form of ($QQDQQ$). Particle timing information is given by the scintillation counters. Incident kaons are identified by a velocity selective Cerenkov detector (Ck) and by time-of-flight measurement between two scintillation counters; one ($S1$) in front of the kaon spectrometer and another ($S2$) in front of target. Reaction pions are identified by time of flight alone between $S2$ and two scintillation counters ($S3$,$S4$) behind the pion spectrometer. A scintillation hodoscope is positioned around the target to tag the hypernuclear events by their decay particles, Fig. 2. This decay detector consisted of four veto scintillation counters in front of an array of lead-scintillation shower counters. The shower counters are divided into three layers with independent readout of each layer. The array was five radiation lengths in total thickness. Each layer had eight pieces of 3.2 mm scintillator and seven pieces of 4.2 mm Pb in a sandwich attached to a light guide. Approximately 0.55 cm of Pb is placed between the veto-counter and shower-counter array to initiate a shower. The operation and efficiency of the decay detector including solid angle coverage will be discussed in the Appendix.

Data were collected at two different scattering angles, effective spectrometer angles of 4° and 12°, using ^{12}C and ^{7}Li targets with sizes of $7.6\times4\times2$ and $7.6\times4.6\times6$ cm^3. These targets were about 2g/cm^2 in thickness. The momentum of the incident kaons was chosen as 715 MeV/c corresponding to 130–150 MeV/c momentum transfer to Σ. A maximum in the elementary cross section for the $p(K^-,\pi^+)\Sigma^-$ occurs near this momentum.[13] Below 715 MeV/c kaon momentum the rate drops rapidly. The central momentum of pion spectrometer was set at 556 MeV/c which enables one to measure missing mass near the Σ^--nucleus threshold region for all targets.

The absolute binding-energy scale was obtained after correcting for the energy loss in both the spectrometers and the target. A calibration measurement of straight through beam at 715 MeV/c (K) and 556 MeV/c (π) with and without the target was used to determine the energy loss due to the $\frac{1}{2}$-in scintillation counter $S2$ backed by a piece of $\frac{1}{2}$-in polyethylene, located between the rear side of the kaon spectrometer and the target. The backing was used as a resolution monitor during the data collection.

The spectrometer acceptance as a function of hypernu-

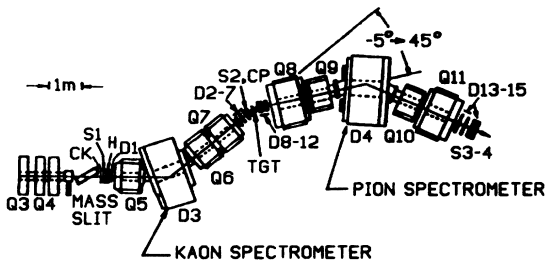

FIG. 1. Experimental layout of the hypernuclear spectrometer and LESBI line at the AGS.

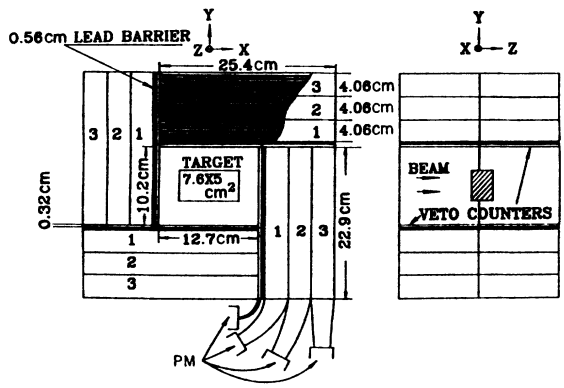

FIG. 2. The decay detector with four veto counters and 24 shower counters.

clear binding energy was also measured by free sigma production in the $^1H(K^-,\pi^+)\Sigma^-$ reaction using a polyethylene target. Only data in the region where the acceptance corrections were less than 30% were used. This provided a momentum bite corresponding to about 50 MeV in binding energy. The free sigma peak with the known $^1H(K^-,\pi^+)\Sigma^-$ cross section[13] also provided a convenient method for determining the cross section for the $^{12}_{\Sigma}$Be and $^{7}_{\Sigma}$H production. The width of this peak as produced from the scintillation counter $S2$ was observed to be 2.5 MeV FWHM. By an appropriate reaction vertex cut in the target position, reactions from this counter can be removed from the final data.

In addition, the ^{7}Li target used in the 4° measurement had a significant hydrogen contamination on the surface which caused a free Σ peak in the missing mass spectrum. This Σ peak was used to correct the absolute binding energy scale. The correction was made by measuring the Σ peak location (including energy loss) in the missing mass spectrum using hydrogen target kinematics.

The peak disappeared in the spectra at 12° after the target surface was cleaned. It was removed from the 4° data by fitting it to a Gaussian shape and substracting it from the spectrum. This peak as obtained from the untagged data under the assumption of a linear background is replotted in Fig. 3 to illustrate the experimental resolution.

The final correction for the pion spectrometer acceptance was made using the result given in the measurement of the $^1H(K^-,\pi^+)\Sigma^-$ cross-section calibration. To avoid large error, only data in a region of 10 to -40 MeV hypernuclear binding energy were used. In this region the acceptance is always higher than 70%.

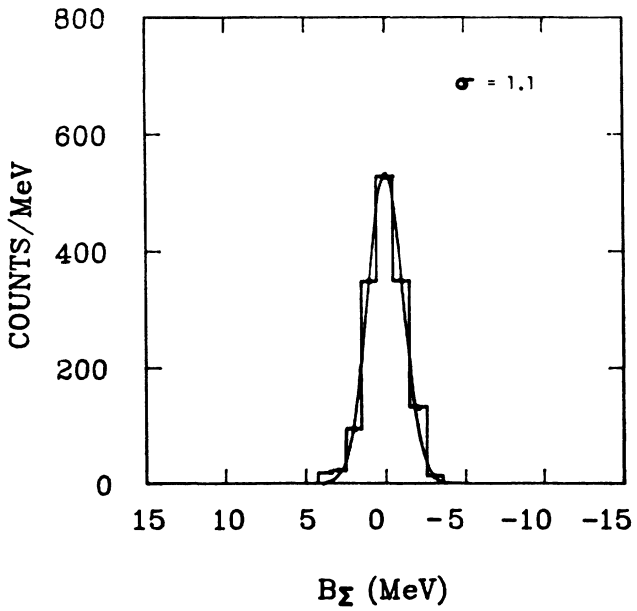

FIG. 3. The π^+ spectrum from the $^1H(K^-\pi^+)\Sigma^-$ reaction on hydrogen on the surface of the target. The experimental resolution is shown to have a $\sigma = 1.1$ MeV.

III. DATA ANALYSIS

The experimental data for the (K^-,π^+) reaction on ^{12}C and ^{7}Li targets at both 4° and 12° were analyzed to obtain the hypernuclear missing mass spectrum as a function of the hypernuclear binding energy. The hypernuclear binding energy was calculated by

$$E = [(\omega + MA)^2 - q^2 - MHy]^{1/2} ,$$

where ω and q are the energy and momentum transfers in the $A(K^-,\pi^+)Hy$ reaction, respectively. MA is the target mass, and MHy is the hypernuclear mass at threshold.

The analysis of the hypernuclear spectra without the decay hodoscope tag was quite straightforward. The data were corrected using the computer program RAYTRACE which used the position and angles of the entrance and exit tracks in the spectrometers to improve the resolution and remove background events. If the target vertex cut is placed about $S2$, a peak from $^1H(K^-,\pi^+)\Sigma^-$ is present which was used for calibration and a resolution monitor. The resulting spectra are then corrected for spectrometer acceptance and detector efficiency. These spectra are plotted in Figs. 4 and 5.

The decay tag was implemented by separating events using the veto scintillator into charged and neutral decay modes. Events without any energy deposition in the decay detector were caused by incomplete detector acceptance. The neutral mode with large pulse height in the shower detector was identified as a π^0, which occurs from the Λ decay in $\Sigma N \rightarrow \Lambda N$ conversion. In the case of the charged decay mode one can separate pion decay of a Λ by use of the Monte Carlo distribution function as described in the Appendix. The tagged spectra are plotted in Figs. 6 and 7.

IV. RESULTS AND CONCLUSIONS

The resulting spectra corrected for spectrometer acceptance and binned in 1-MeV intervals with respect to the sigma binding energy are shown in Figs. 4–7. Errors in the data are presented as statistical only. The solid curves in the spectra represent a calculation, without inclusion of experimental resolution, for Σ production from p and s shell protons in the targets, producing a free Σ with no Σ-nucleus interaction in the final state. The difference between these curves and the data are therefore due to the Σ-nucleus interaction. The p- and s-wave Σ production are independently normalized to the data and the s-hole excitation in the ^{6}He nuclear core was chosen to be 15 MeV, although the strength should be distributed over several states in ^{6}He. The ratio of the p- to s-hole strength and energy splittings are close to that published for the Λ hypernuclear system.[14] The Σ conversion decay mode (denoted hereafter as the strong-decay mode) is dominant, but becomes less probable as the recoil velocity of the Σ increases. Stated differently, the signal gated by the strong-decay tag decreases more rapidly than the ungated signal as the binding energy decreases, tending to suppress the quasifree region of the spectrum.

The $(\Sigma^- + {}^{11}B)$ spectrum shows a large enhancement near threshold. The spectra are reminiscent of final-state

interaction enhancements. In particular, the $(\Sigma^- + {}^{11}B)$ spectrum is very similar to a continuum shell-mode calculation[15] which has enhancements but no narrow (~ 2 MeV) states. In addition, while there is significant reaction strength below sigma threshold, there is no evidence in either the tagged or untagged data of narrow structure (~ 2 MeV) in this region. The tagged data can be directly compared to the tagged stopped K^- data of Ref. 8 if the latter data are rebinned at 1-MeV intervals. This comparison is made by observing the deviation from zero in the difference between the two spectra. A χ^2 test of this difference produces a value of 1.4 per degree of freedom for 14 degrees of freedom over the binding-energy interval from 0 to approximately 16 MeV. Quoted statistical errors and arbitrary normalization are used. Comparison of these data to the in-flight data[7] is somewhat more tenuous because of the large difference in momentum transfer. However, if the tagged spectra,

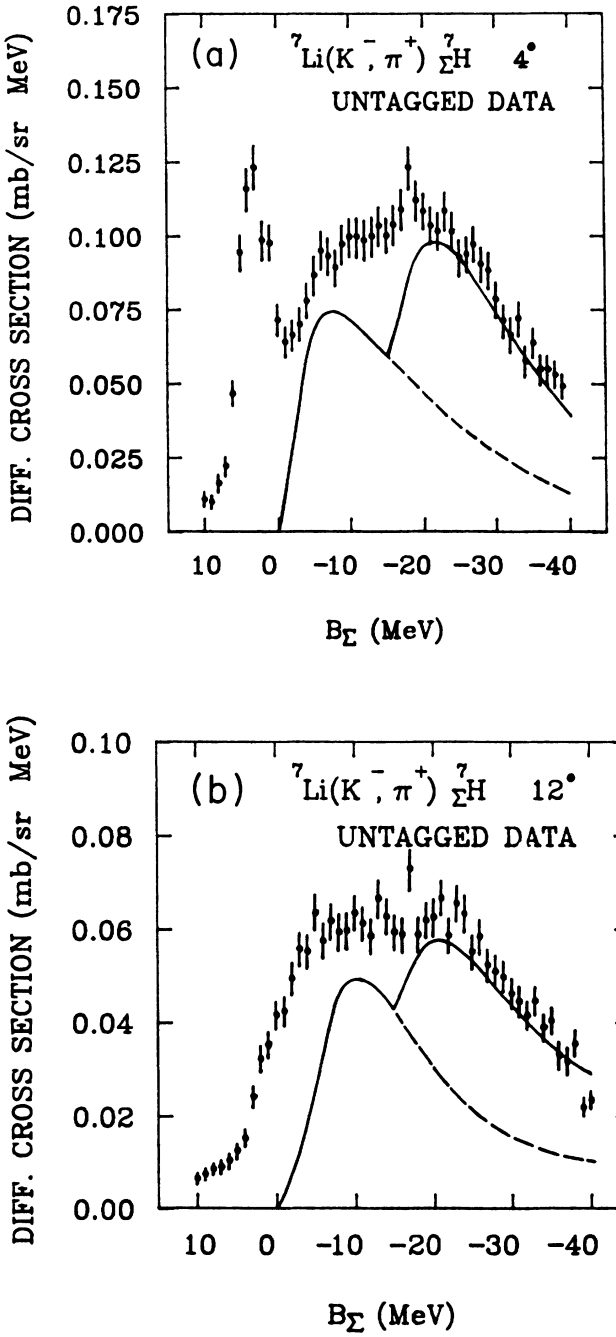

FIG. 4. Untagged spectra of the system $\Sigma^- + {}^6$He at the angles of 4° and 12°. The peak in the spectrum is due to ^{1}H$(K^-\pi^+)\Sigma^-$ on hydrogen (see Fig. 3).

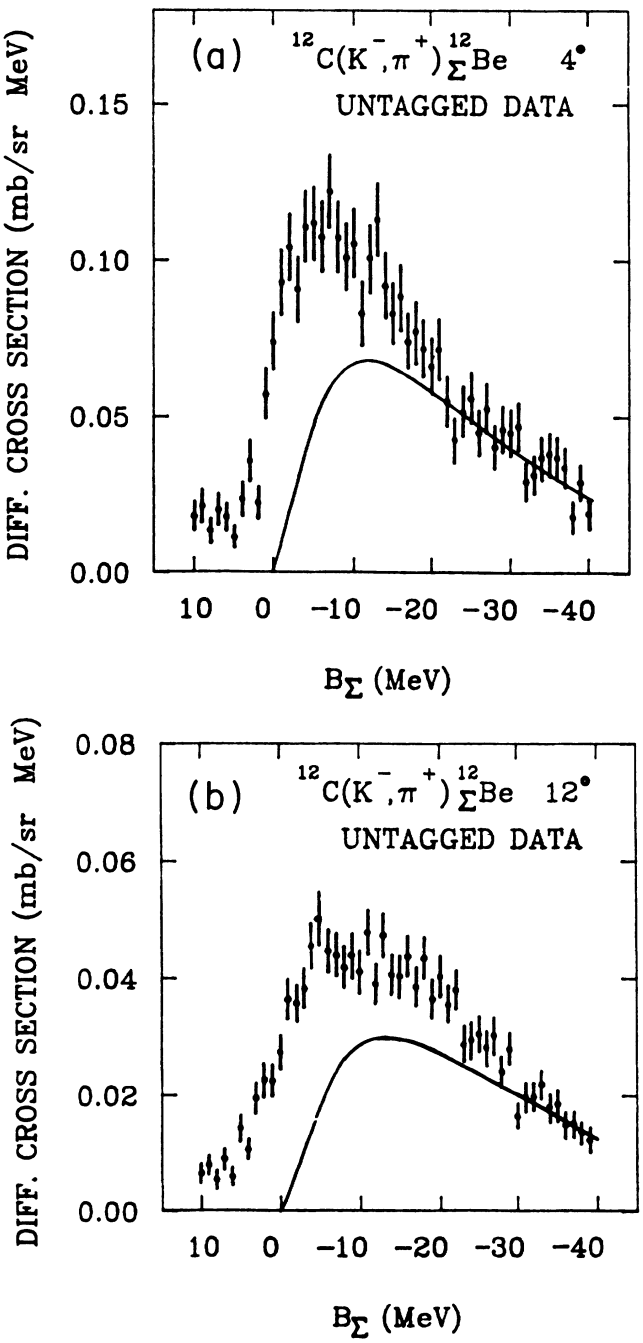

FIG. 5. Untagged spectra of the system $\Sigma^- + {}^{11}$B at the angles of 4° and 12°.

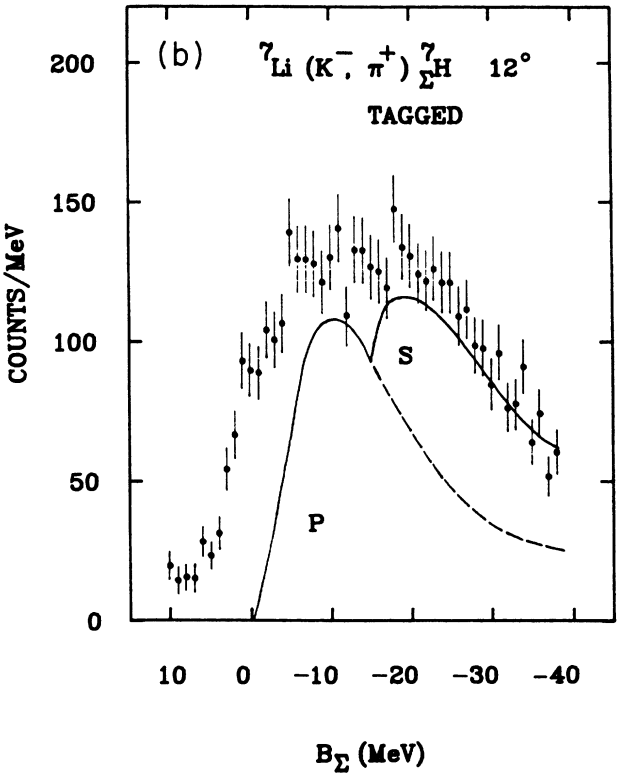

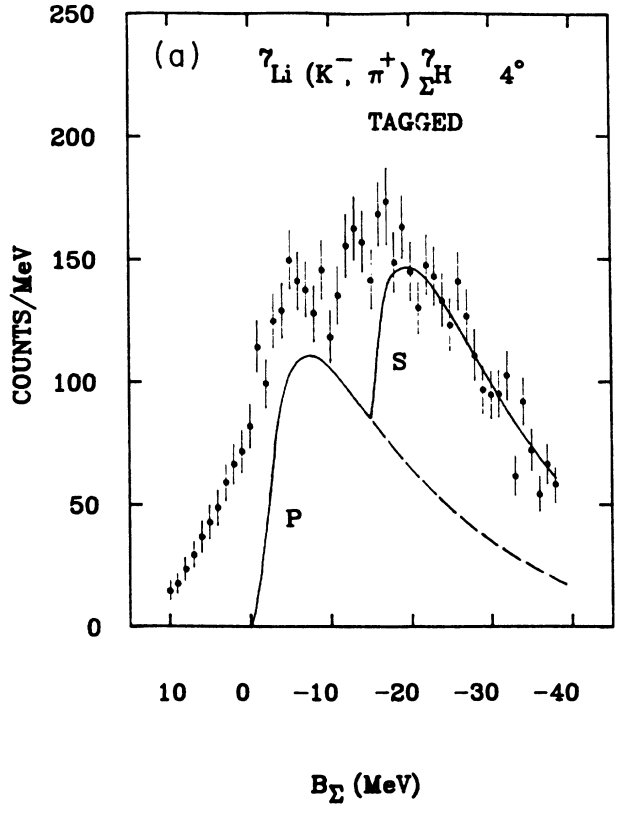

FIG. 6. Spectra tagged by the strong-decay mode for the system $\Sigma^- + {}^6$He.

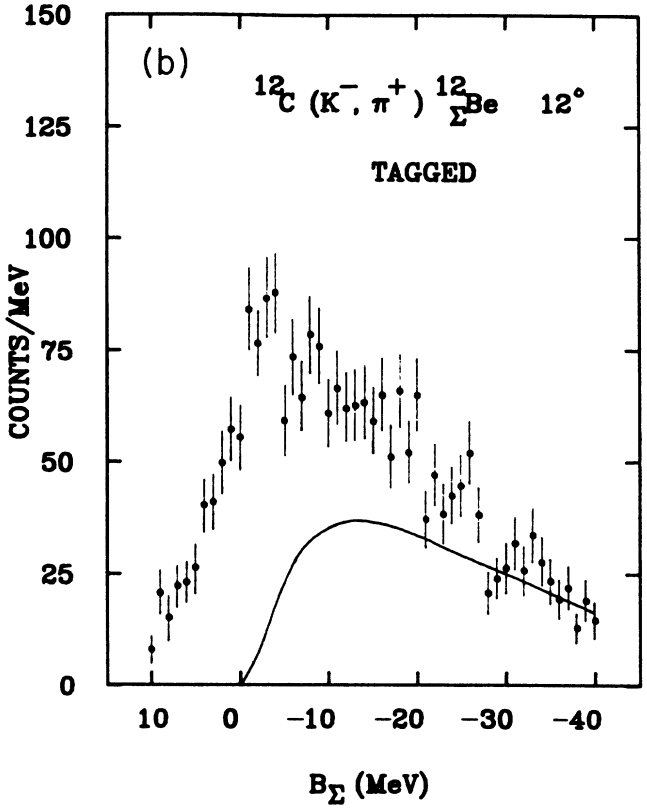

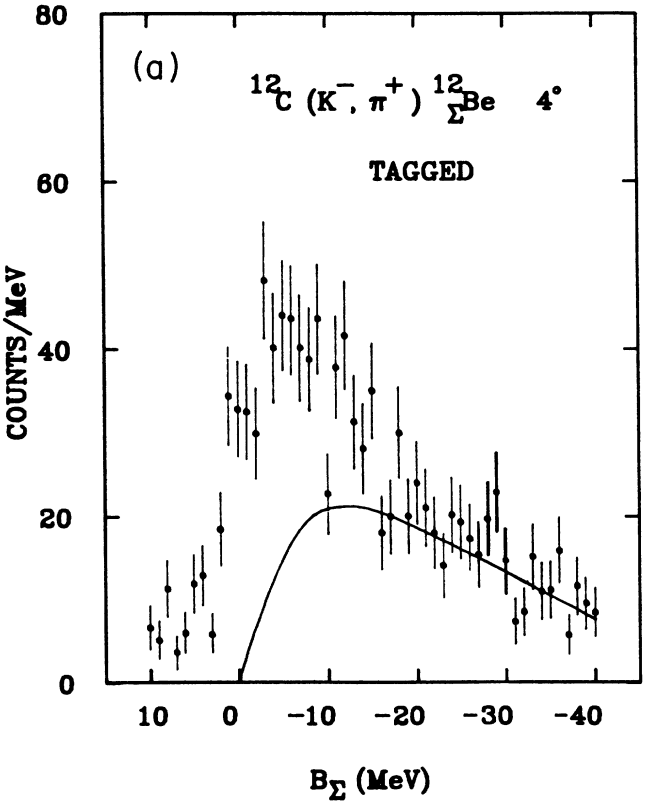

FIG. 7. Spectra tagged by the strong-decay mode for the system $\Sigma^- + {}^{11}$B.

which tend to suppress the quasifree region of the spectrum, are used, a similar calculation yields a χ^2 per degree of freedom of 2.5 over the same binding-energy interval. Visually all the data of both Refs. 7 and 8 are similar to the present experiment.

The importance of proper calculation of the "quasifree" production has been previously emphasized.[16] The quasifree shape can be found by combining the free Σ production, as calculated above, with a Σ-nucleus final-state interaction. This shape follows the average shape of the enhancements in all the data and must be carefully subtracted in order to observe any remaining narrow structure. However, the characterization of continuum structure as opposed to background is then ambiguous. A theoretical representation of the data is best done in a continuum shell model which avoids these problems.[15]

The shape of the spectra at 4° compared to 12° changes slightly. This is most likely due to the larger momentum transfer which introduces *s*-shell substitutions 20 Mev or so above threshold, although the *p* shell still dominates. If the narrow peaks seen in the data of Ref. 8 are real and correspond to $p_{3/2}$ and $p_{1/2}$ states, then one should expect to see a significant strength change in the $^{7}_{\Sigma}$H spectra several MeV above threshold.[11] This is not observed in our data.

The $(\Sigma^- + {}^6\mathrm{Li})$ continuum spectrum is in many respects similar to the $^{6}_{\Sigma}$H continuum spectrum obtained in a previous BNL experiment[6] except that the enhancement higher in the continuum [assigned as $(1s_p^{-1}, 1s_\Sigma)$] is not as prominent. The more recent interpretation[16] indicates that much of this structure can be assigned to quasifree Σ production. In all of these spectra there is no evidence for narrow structure ($\sim$2 MeV) below threshold.

In conclusion, the results of this experiment cannot confirm the existence of the narrow discrete structure seen in the data of the stopped K^- experiments on ^{12}C. However, there is a broad enhancement just *above* the sigma threshold. The spectra do not have the expected momentum transfer dependence for a simple substitutional transition and the spectrum shape is not consistent with a shell-model calculation of sigma continuum resonances including residual interactions. The spectra are consistent with a final-state interaction calculation. Therefore, simple structure assignments based on narrow, particle-hole substitutional states are probably not possible. Finally, in all spectra there is no evidence for narrow structure ($\sim$2 MeV) below the sigma threshold which should be observed if Σ conversion widths are significantly suppressed.

ACKNOWLEDGMENTS

The authors gratefully acknowledge the staff support of AGS and BNL. This work was supported in part by the U.S. Department of Energy under Grant Nos. DE-AS05-76ERO and DE-AC02-76CH00016.

APPENDIX: MONTE CARLO SIMULATION OF THE DECAY DETECTOR

A Monte Carlo simulation of the decay detector was used to predict (1) the momentum range and the angular distribution of all the decay particles, (2) the energy deposition in the decay detector, and (3) the detector efficiency.

This simulation was based on either a hypernuclear decay due to $\Sigma N \rightarrow \Lambda N$ conversion following the chain:

$$A(K^-,\pi^+)[(A-1)+\Sigma^-] \rightarrow [(A-2)+N+\Lambda] \rightarrow [(A-2)+N+p+\pi^-] \quad \text{or} \quad (A1)$$

$$[(A-2)+N+p+\pi^0] \rightarrow [(A-2)+N+p+\gamma+\gamma]$$

or a weak Σ^- decay of the form

$$A(K^-,\pi^+)[(A-1)+\Sigma^-] \rightarrow [(A-1)+N+\pi^-] \, . \quad (A2)$$

Here A stands for the target nucleus.

In the hypernuclear decay, the reaction $A(K^-,\pi^+)[(A-1)+\Sigma^-]$ was considered as a two-body reaction with the recoil mass formed by $[(A-1)+\Sigma^-]$. The Σ-Λ conversion then followed as a three-body reaction, e.g., the Σ^- interacts with a proton inside the nucleus and forms a three-body system $[(A-2)+N+\Lambda]$, where $(A-2)$ is the residual mass number. The branching ratio for Λ decay is taken from the free value. It is also assumed that π^0 decays into 2γ's with a 100% branching ratio. In the weak-decay mode, the Σ was considered as a free particle because of the relatively large momentum transfer (about 130–150 MeV/c), e.g., a direct three-body reaction. Disregarding the Σ atomic recapture process, the free Σ^- decay should have a π^- and a neutron in the final state.

However, a Σ^- may also decay through $\Sigma N \rightarrow \Lambda N$ conversion in an atomic recapture process on another target nucleus.[17] The recapture process will vary with different targets and create a background of decays that cannot be completely removed from the tagged data. From Ref. 17 it is expected that about 50% of the Σ^- will undergo nuclear conversion in the parent nucleus and 50% of those Σ^- which are emitted as quasifree particles will decay in flight. Thus a probability of 25% ($0.5 \times 50\%$) will be misidentified as strong rather than weak decays.

Only the final-state decay particles n, γ, p, and $\pi^{\pm}$ are visible in the shower detector. Because of the small thickness of the veto scintillator (3.2 mm), neutron detection in the veto counters is negligible. The decay neutrons can interact in the shower detector but the probability of significant energy loss in the scintillators is small. Most of the decay protons (momentum $\leq$200 MeV/c) are stopped in the target due to large ionization energy. A few protons could escape from the target and stop in the Pb layer after penetrating the veto counter. Even though the decay neutrons and protons are not considered in the Monte Carlo analysis, they caused no significant effect within the energy range for the Monte Carlo fit. The most efficiently detected final-state particles are the γ's and π's.

The veto counter identifies a charged particle decay mode. In neutral event, only two photons (in the 30–200 MeV energy range) from a π^0 decay can be efficiently

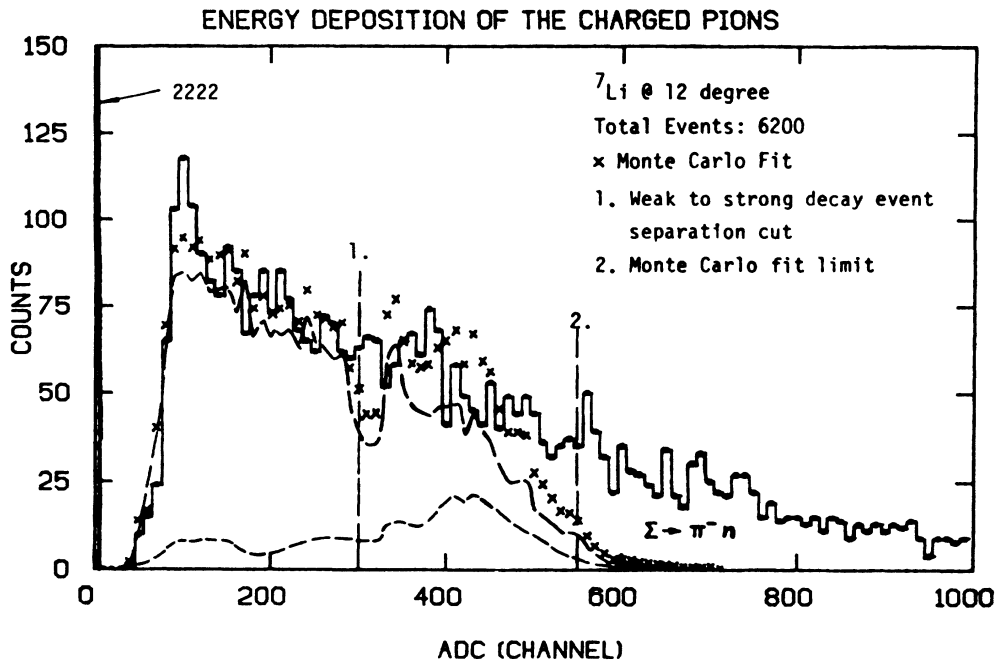

FIG. 8. A Monte Carlo fit to the experimental charged pion spectrum measured in the shower counter for the ^{7}Li target at 12°.

detected by the shower process. The thickness of the shower counters insures almost all the penetrating photons are showered. In a charged particle event, the decay proton leaves most of its energy in the veto counter, causing a large pulse height, and stops in the lead layer before the shower detector. Pions either stop in the shower counter or penetrate through the detector. Each of the layers in the decay detector was calibrated using a β/γ source (average energy deposition about 0.5 MeV) and by cosmic ray muons which leave about 4 MeV energy in each shower counter.

The Monte Carlo calculation demonstrates that the momentum range of the photons is between 30–200 MeV/c, so that the five radiation lengths of shower-counter array ensured nearly all the photons showered inside the detector. The Monte Carlo angular distribution of these photons was used to determine the solid angle coverage of the shower detector. In the detector, γ showers were identified by absence of a signal in the veto detector and a total energy above threshold deposited in the shower counter. These can only be Λ decay events, so that the detection of these photons was important for confirmation of the tagged spectrum shape. The maximum total shower energy deposition was approximately 30 MeV.

The Monte Carlo simulation also tracked the charged particles through the decay chains of Eqs. (A1) and (A2). The experimental momentum and spatial distribution of the beam, the target thickness, and the geometry and composition of the detector were all included in the simulation.

The momentum of the hypernuclear decay pions (π^0 and π^- from Λ decay) ranges from 40 to 180 MeV/c. In comparison to this, the weak-decay pions are more energetic (in range of 130—240 MeV/c). Some of these later pions can penetrate the shower detector. The difference in the energy deposition of the pions from the two decay modes provides a means, in addition to a γ shower, to specify the decay channel. The Monte Carlo spectra can then be used as energy distribution functions of the two different decay modes for charged particle events. Thus by fitting the experimental energy spectra one can check the Monte Carlo predicted π^0 detection efficiency using the Λ decay branching ratio, as well as determine the branching ratio for the decay channels given by Eqs. (A1) and (A2). Thus the experimental energy deposition was fit by the summed Monte Carlo prediction in the energy between 0 and 22 MeV (0 to channel 560) by varying the total number of Σ's and Λ's which decay by π^- emission for each target and angle. Events with energy deposition higher than 22 MeV (marked by the vertical line labeled 2 in Fig. 8) are mainly from π^- interacting in the detector. These are not included in this simulation. Figure 8 shows the experimental energy spectra for the charged decay modes for the ^{7}Li targets at 12°, the Monte Carlo fits are shown by x's in the figures. The dashed lines indicate the contributions from the two possible decay modes. Because of the pions which interact in the detector only the strong-decay mode can be extracted from the data with confidence. The other spectra and fits are similar. Thus the spectrum shape for strong decay is determined by all events with energy deposition less than the weak- to strong-decay cut marked by the vertical line labeled 1. The spectrum sample, tagged as charged pion decay from Λ's, was identical within statistics to the sample obtained tagged π^0 decay. The spectra still contains some events due to free Σ^- capture on other target nuclei. The shape changes due to these events will be relatively small.

The remaining correction for the charged event data was for the solid angle acceptance. By Monte Carlo simulation, about 80% of 4π for the charged event modes was obtained.

[1]R. H. Dalitz and A. Gal, Ann. Phys. (N.Y.) **116**, 167 (1978).
[2]Brookhaven National Laboratory experiment No. 798, 1985 (unpublished); R. E. Chrien and E. V. Hungerford, Proceedings of the Continuous Electron Beam Accelerator Facility Summer Workshop, edited by F. Gross and C. Williamson (SURA, Newport News, VA, 1987), p. 402.
[3]D. J. Millener, A. Gal, C. B. Dover, and R. H. Dalitz, Phys. Rev. C **31**, 499 (1985).
[4]A. Gal and C. B. Dover, Phys. Rev. Lett. **44**, 379 (1980).
[5]R. Bertini *et al.*, Phys. Lett. **90B**, 375 (1980).
[6]H. Piekarz *et al.*, Phys. Lett. **110B**, 428 (1982).
[7]R. Bertini *et al.*, Phys. Lett. **136B**, 29 (1984).
[8]T. Yamazaki *et al.*, Phys. Rev. Lett. **54**, 102 (1985).
[9]W. Bruckner *et al.*, Phys. Lett. **79B**, 157 (1978).
[10]C. B. Dover, A. Gal, and D. J. Millener, Phys. Rev. Lett. **56**, 119 (1986).
[11]C. B. Dover and A. Gal, Phys. Lett. **110B**, 433 (1982).
[12]P. Pile, Nucl. Phys. **A450**, 517 (1986).
[13]G. P. Gopal, Nucl. Phys. **B119**, 362 (1977).
[14]R. Bertini *et al.*, Nucl. Phys. **A368**, 365 (1981).
[15]M. Kohno, *et al.*, Nucl. Phys. **A470**, 609 (1987); R. Wunsch and J. Zofka, Phys. Lett. B **193**, 7 (1987).
[16]R. E. Chrien, E. V. Hungerford, and T. Kishimoto, Phys. Rev. C **35**, 1589 (1987).
[17]C. Vander Velde-Wilquet *et al.*, Nucl. Phys. **A241**, 511 (1975).

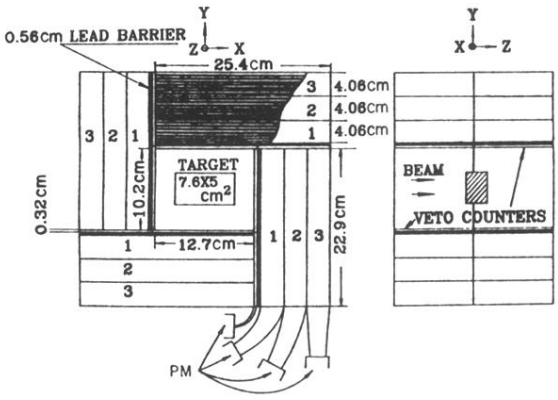

FIG. 2. The decay detector with four veto counters and 24 shower counters.